TRANSONIC COMPUTATIONS ABOUT COMPLEX CONFIGURATIONS USING COUPLED INNER AND OUTER FLOW EQUATIONS

Uno G. Nävert and Yngve C-J. Sedin

SAAB-SCANIA AB
Saab Aircraft Division
Computational Aerodynamics
Linköping, Sweden

Abstract

Modern aircraft, in particular fighters, are characterized by a high degree of geometrical complexity. To master such complicated geometries in transonic computations, one often has to rely on small disturbance (TSP) formulations on Cartesian grids. Wing boundary conditions are then easily imposed using thin-wing theory while fuselage boundary conditions usually are more difficult to implement. This paper presents a numerical method for solving the TSP equation about a complex slender configuration emphasizing a consistent treatment of the boundary conditions on the fuselage surface. The basic concept is a decomposition in two coupled inner and outer problems using the theory of matched asymptotic expansions. The outer problem is discretized using a standard 3D finite difference scheme. The inner problem, enforcing the fuselage boundary conditions, is solved as a sequence of cross-flow problems using a linear 2D panel method. Several test runs on a CRAY-1 computer have demonstrated the reliability and robustness of the above procedure. Computed pressure distributions for a number of 3D cases, including one of fighter type, are in good agreement with wind tunnel test data.

1. Introduction

In practical aerodynamic design and analysis work there is a wide scale of methodological needs ranging from linear panel methods up to more elaborate non-linear techniques. Although in recent years great progress has been made to Euler and Navier-Stokes methods[6][8], they still are complicated and expensive to operate in 3D for most every day engineering work. In particular, they require an efficient and flexible grid generation process that still has to be invented to cover all different details of an aircraft in a rapid and efficient way.

Two decades ago, Woodward[15], among others, developed a panel method that became a widespread tool in many aircraft industries. With this simple but flexible method a large variety of aerodynamic problems could be tackled includinge e.g. wing-body combinations, external stores, and static aeroelasticity[5]. The results obtained gave qualitative and quantitative guidelines for many aerodynamic problems and opened up the use of computational aerodynamics in practise.

Recalling the rapid evolution of non-linear computational methods during the seventies[7], it should now be possible to develop a similar practical method as flexible and accessable as Woodward's but now including also non-linear transonic flow. Steps in this direction were taken earlier e.g. by Boppe[4]. The present paper is aiming at the same goal but the approach is somewhat different.

One key feature to the success of the Woodward-type panel method was the simple treatment of the boundary conditions which were applied on mean surfaces or interference shells. This enabled rapid and flexible changes of the geometry without having to repanel the computed object. The background to this of course lies in the small disturbance assumption. Hence, using the same philosophy in non-linear transonic flow we are led to the transonic small perturbation (TSP) formulation that would give us a similar flexibility.

A numerical example shown in this paper indicates that a TSP formulation, even for a relatively thick airfoil in 2D, gives results well within engineering accuracy compared to full potential or Euler solutions. This is if the boundary conditions are properly treated and higher order terms are correctly implemented.

The present method utilizes the fact that in transonic flow the lateral interaction is very stiff and almost incompressible. Hence, an inner linear cross-flow equation is coupled to an outer non-linear TSP equation using the theory of matched asymptotic expansions[2]. This coupling is fulfilled along a rectangular parallelepiped enclosing the aircraft fuselage. The boundary conditions on lifting surfaces are imposed on mean surfaces. Thus, a flexible method is found for complicated configurations using a simple cartesian grid for the outer flow.

The method is capable of handling fighter type configurations including lifting surfaces, fuselage with canopy and air intake, and a vertical fin. External loads will be incorporated in the near future. Techniques using local grid refinements are also studied and a convenient data structure for this has been found.

Efforts to incorporate fuselage effects using a linear panel method were reported earlier[14]. However, the interactive transonic coupling of inner and outer flow fields was not considered.

2. Basic Concept: Coupled Inner and Outer Problems

We shall consider three-dimensional flow about a combination of a thin wing, W, and a slender body mounted on a sting, B, at a small angle of attack, α, relative to a subsonic free stream of velocity U_∞ and Mach number M_∞ close to unity. The configuration is symmetric with respect to the xz-plane of a Cartesian coordinate system (x,y,z) having its x-axis aligned with the longitudinal axis of the body, cf. Figure 1.

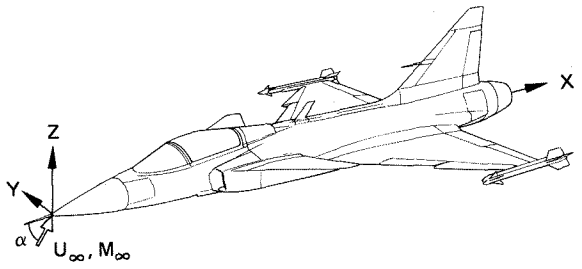

Figure 1. Cartesian coordinate system.

Assuming irrotational flow we introduce the velocity potential Φ and the disturbance potential ϕ related by

$$\Phi=U_\infty[x\cos\alpha+z\sin\alpha+\phi]. \tag{1}$$

Normalizing to $U_\infty=1$ the local Mach number M for small disturbances is given by[10]

$$M^2=M_\infty^2+M_\infty^2(3-(2-\gamma)M_\infty^2)\phi_x. \tag{2}$$

Here $\gamma=1.4$ is the specific heat ratio.

For an isolated wing of thickness ratio $\tau_w \ll 1$ thin wing theory gives[2]

$$T\phi\equiv(1-M^2)\phi_{xx}+\phi_{yy}+\phi_{zz}=O(\tau_w^{4/3}). \tag{3a}$$

Close to the wing this relation can be simplified to

$$\phi_{zz}=O(\tau_w^{4/3}). \tag{3b}$$

For an isolated body of thickness ratio $\tau_b \ll 1$ slender body theory gives

$$T\phi=O(\tau_b^2), \tag{4a}$$

or, close to the body,

$$L\phi\equiv\phi_{yy}+\phi_{zz}=O(\tau_b^2). \tag{4b}$$

Let us define an infinite parallelepiped P, with edges parallel to the x-axis, encompassing the body and the innermost part of the wing. The interior and exterior of P outside W and B is denoted by P^i and P^e, respectively. Motivated by equation (3) and (4) we now require the disturbance potential ϕ for the wing/body combination to satisfy

$$T\phi=0 \quad \text{in } P^e, \tag{5a}$$

$$L\phi=0 \quad \text{in } P^i. \tag{5b}$$

These outer and inner equations are coupled via compatibility conditions on the surface ∂P of P, where ϕ and its normal derivative ϕ_n are required to be continuous, cf. Figure 2.

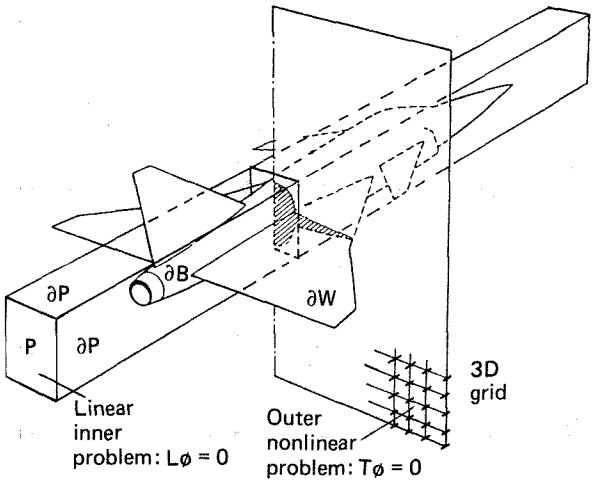

Figure 2. Coupled inner and outer problems.

To formulate boundary conditions for the wing we write the equation satisfied by a point (x,y,z) on the wing surface ∂W as

$$z - Z(x,y) = 0 \quad \text{on } \partial W,$$

where Z(x,y) denotes one of the two functions $Z^-(x,y)$ and $Z^+(x,y)$ defining the lower and upper wing surface, respectively. The tangential flow boundary condition is then given by

$$\nabla\Phi\cdot(-Z_x,-Z_y,1)=0 \quad \text{on } \partial W,$$

or, using (1) with $|\alpha|\ll 1$,

$$\phi_z=(1+\phi_x)Z_x+\phi_y Z_y-\alpha \quad \text{on } \partial W. \tag{6}$$

As suggested by (3b), outside P this condition is imposed on a plane mean surface ∂W^0 at a constant $z=Z^0$ rather than on the physical wing surface ∂W. Equation (5a) is then extended to hold in P^0 defined as the exterior of P outside ∂W^0. It is important to keep the term $(1+\phi_x)$ multiplying Z_x in (6), c.f. Section 6 below.

The potential ϕ is continuous except in points (x,y,Z^0) on the wake downstream of ∂W^0. Here the Kutta condition admits potential jumps equal to the circulation $\Gamma(y)$, i.e., potential jumps which do not depend on x. The circulation distribution $\Gamma(y)$ is given by the difference in potential between the upper and lower wing surfaces at the trailing edge.

The tangential flow condition on the body surface ∂B is given by

$$\nabla\Phi\cdot(n_x,n_y,n_z)=0 \quad \text{on } \partial B,$$

where (n_x,n_y,n_z) is the outward unit normal on the body surface. Expressing this as a condition for the normal derivative ϕ_n given by

$$\phi_n \equiv (\phi_y,\phi_z)\cdot(n_y,n_z)/\sqrt{n_y^2+n_z^2} \quad \text{on } \partial B,$$

we obtain, using (1) with $|a|<<1$ and $|\phi_x|<<1$,

$$\phi_n = h(x,y,z) \equiv (-n_x - a n_z)/\sqrt{n_y^2+n_z^2} \quad \text{on } \partial B. \qquad (7)$$

This type of condition is also used on that part of the wing surface ∂W which is inside P.

In the far field, except for Trefftz' plane, we impose Dirichlet boundary conditions $\phi=g$ with g given by the expressions derived by Klunker[9] for a thin wing. In Trefftz' plane Π given by

$$\Pi \equiv \{(x,y,z): x=\text{constant}\to\infty\}$$

representing downstream infinity we decompose ϕ as $\phi=\phi'+\phi''$. Here $\phi'=g$ is given by Klunker's expressions and ϕ'' represents the influence of the body. To determine ϕ'' we solve $L\phi''=0$ in Π with the boundary condition $\phi''=h-g$, cf. (7), imposed on the sting contour. The function g depends on the circulation Γ and has to be updated during the solution process.

3. Discretization

The outer and inner problems introduced in the previous section are restricted to finite computational domains $D^o \equiv P^o \cap D$ and $D^i \equiv P^i \cap D$, where D is defined by

$$D \equiv \{(x,y,z): x_{min} \le x \le x_{max}, 0 \le y \le y_{max}, z_{min} \le z \le z_{max}\}.$$

The far field boundary conditions are imposed on the boundary ∂D of D as described in Section 2.

We shall now in turn discuss discretization in D^o, in D^i, and in Trefftz' plane Π at $x=x_{max}$. We denote the inner solution, i.e., the restriction of ϕ to D^i, by $\psi=\psi(x;y,z)$ to emphasize the two dimensional character of the inner problem.

Discretization of the outer problem

The outer problem is given by

$$T\phi = (1-M^2)\phi_{xx}+\phi_{yy}+\phi_{zz}=0 \quad \text{in } D^o, \qquad (8a)$$

$$\phi_z = (1+\phi_x)Z_x+\phi_y Z_y - \alpha \quad \text{on } \partial W^o, \qquad (8b)$$

$$\phi_n = \psi_n \quad \text{on } \partial P \cap D, \qquad (8c)$$

$$\phi = g \quad \text{on } \partial D \cap P^o. \qquad (8d)$$

The governing non-linear operator T is of mixed type being elliptic in subsonic regions (M<1) and hyperbolic in supersonic regions (M>1). The right hand sides of the boundary conditions all depend on the solution and must be determined iteratively. This procedure is discussed in Section 5.

Equation (8a) is discretized using Murman's type-dependent fully conservative scheme[11] on a Cartesian grid, see Figure 3.

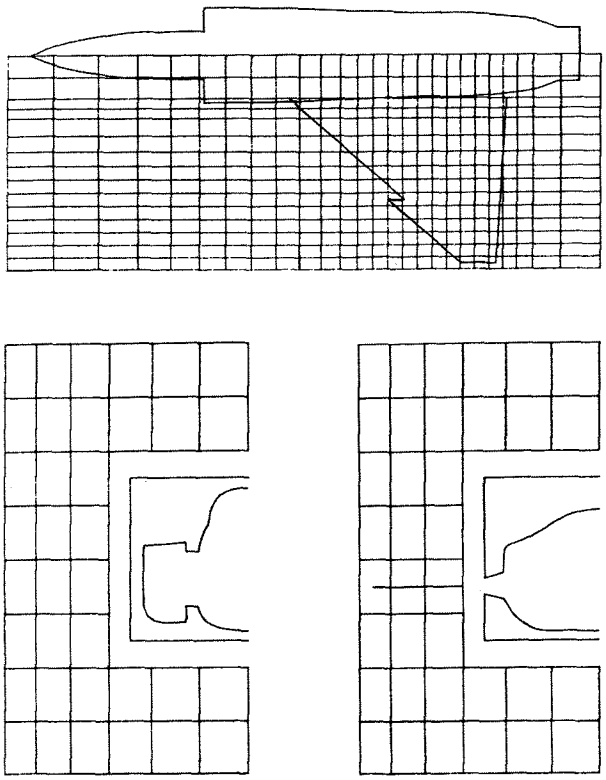

Figure 3. Example of cartesian computational grid in the wing plane and in two cross cuts containing air intake and wing.

Below we give the resulting difference equations for a uniform grid indexed by i,j,k with grid size $\Delta x,\Delta y,\Delta z$, i.e., $\phi_{ijk}=\phi(i\Delta x,j\Delta y,k\Delta z)$. We use the convention that indices which are omitted have the value i,j, or k, i.e., $\phi_{i+1}=\phi_{i+1,jk}$ and so on. With

$$s_{ijk} \equiv 1-M_\infty^2-M_\infty^2(3-(2-\gamma)M_\infty^2)(\Delta x)^{-1}(\phi_{i+1}-\phi_{i-1})/2,$$

$$\mu_{ijk} \equiv 0 \text{ if } s_{ijk}>0 \quad \text{(subsonic flow)},$$
$$\mu_{ijk} \equiv 1 \text{ if } s_{ijk}<0 \quad \text{(supersonic flow)},$$

$$p_{ijk} \equiv s_{ijk}(\Delta x)^{-2}(\phi_{i-1}-2\phi_i+\phi_{i+1}),$$

$$q_{ijk} \equiv (\Delta y)^{-2}(\phi_{j-1}-2\phi_j+\phi_{j+1}),$$

$$r_{ijk} \equiv (\Delta z)^{-2}(\phi_{k-1}-2\phi_k+\phi_{k+1}),$$

the difference approximation of (8a) reads

$$(1-\mu_{ijk})p_{ijk}+\mu_{i-1,jk}p_{i-1,jk}+q_{ijk}+r_{ijk}=0. \qquad (9a)$$

We note that upstream differencing is used in the x-direction in case of supersonic flow.

Let (x_i,y_j,Z^o) be a point on the wing mean surface ∂W^o, which is placed halfway between two grid planes indexed by K and K+1, say. The boundary condition (8b) is imposed by defining

$$r_{ij,K} \equiv (\Delta z)^{-1}\{\phi_z-(\Delta z)^{-1}(\phi_K-\phi_{K-1})\},$$
$$r_{ij,K+1} \equiv (\Delta z)^{-1}\{(\Delta z)^{-1}(\phi_{K+1}-\phi_K)-\phi_z\}, \qquad (9b)$$

with ϕ_z taken from (8b). The Kutta condition is

implemented by defining

$$r_{ij,K} \equiv (\Delta z)^{-2}\{\phi_{K-1}-2\phi_K+\phi_{K+1}-\Gamma\},$$

$$r_{ij,K+1} \equiv (\Delta z)^{-2}\{\phi_K+\Gamma-2\phi_{K+1}+\phi_{K+2}\}$$

in points (x_i,y_j,Z^o) on the wake.

Discretization of the inner problem

The inner problem is given by

$$L\psi=\psi_{yy}+\psi_{zz}=0 \quad \text{in } D^i, \tag{10a}$$

$$\psi_n=h \quad \text{on } (\partial B\cup\partial W)\cap D, \tag{10b}$$

$$\psi=\phi \quad \text{on } \partial P\cap D. \tag{10c}$$

This problem has an entirely different character from the outer problem (8) since the governing operator L is linear and two-dimensional.

For each grid plane P_i at $x=x_i$ we discretize (10) in the intersection $D_i\equiv P_i\cap D^i$ using a panel method. The boundary

$$\partial D_i\equiv(\partial B\cup\partial W\cup\partial P)\cap D_i$$

of D_i is replaced by a family of straight panels where each panel has a constant source distribution. Downstream of the wing we also introduce doublet panels along the wake contour $\partial W^o\cap D_i$, see Figure 4.

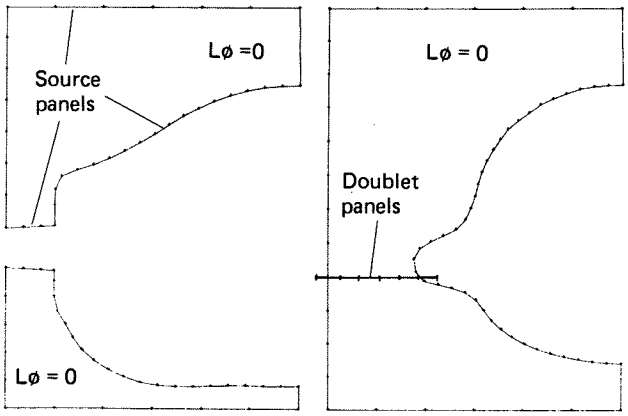

Figure 4. Example of panelling of cross cuts containing wing (left) or wake (right).

The doublet strengths are given by the potential jumps at the wing trailing edge. The source strengths are determined so that the boundary conditions are satisfied in the panel mid points. For each D_i we obtain a dense linear system of equations and the discrete problem can be written

$$A_iS_i=B_i, \quad 1\le i\le imax. \tag{11}$$

Here $\{A_i\}$, $\{S_i\}$, and $\{B_i\}$ denote the system matrices, source strength vectors, and right hand sides, respectively.

Remark: The wing frequently requires a higher resolution power of the grid than is necessary, or even applicable if the the quality of the defining geometry is poor, for the body. In such cases it is sufficient to solve (11) for a subset of $\{i=1..imax\}$ and use a non-oscillatory interpolation procedure[1] to get normal derivatives on ∂P in intermediate planes required in (8c).

Discretization in Trefftz' plane

In Trefftz plane Π we solve the Laplacian problem

$$L\theta=\theta_{yy}+\theta_{zz}=0 \quad \text{in } \Pi\backslash B, \tag{12a}$$

$$\theta_n=h-g_n \quad \text{on } \partial B\ \Pi, \tag{12b}$$

where g and h were introduced in Section 2. This problem is discretized and solved by a panel method as described in the previous subsection. The disturbance potential ϕ in Π is then given by $\phi=\theta+g$.

4. Relaxation Procedure

The discrete outer problem (9) is solved by succesive line over relaxations. In each iteration cycle the grid is swept plane by plane in the x-direction and within each plane line by line in the y-direction with only one line sweep in each plane per cycle.

Let ϕ and ϕ^* denote the potentials before and after one iteration cycle. Further, define an intermediate potential ϕ' by

$$\phi'\equiv\omega^{-1}\phi^*+(1-\omega^{-1})\phi,$$

where ω is the over relaxation factor, below chosen as 1.8. Then ϕ^* is given by[3]

$$(1-\mu_{ijk})p'_{ijk}+\mu_{i-1,jk}p'_{i-1,jk}+q'_{ijk}+r'_{ijk}=0, \tag{13}$$

where in subsonic flow, i.e., $\mu_{ijk}=0$,

$$p'_{ijk} \equiv s_{ijk}(\Delta x)^{-2}(\phi^*_{i-1}-2\phi'_i+\phi_{i+1}),$$

$$q'_{ijk} \equiv (\Delta y)^{-2}(\phi^*_{j-1}-2\phi'_j+\phi_{j+1}),$$

$$r'_{ijk} \equiv (\Delta z)^{-2}(\phi^*_{k-1}-2\phi^*_k+\phi^*_{k+1}),$$

and in supersonic flow, i.e., $\mu_{ijk}=1$,

$$p'_{ijk} \equiv s_{ijk}(\Delta x)^{-2}(\phi_{i-1}-2\phi^*_i+2\phi^*_{i+1}-\phi_{i+1}),$$

$$q'_{ijk} \equiv (\Delta y)^{-2}(\phi^*_{j-1}-\phi^*_j-\phi_j+\phi_{j+1}),$$

$$r'_{ijk} \equiv (\Delta z)^{-2}(\phi^*_{k-1}-2\phi^*_k+\phi^*_{k+1}).$$

Introducing $c\equiv\phi^*-\phi$ we finally rewrite (13) in correction form ending up with a tridiagonal linear system

$$T_ic_{k-1}+T_2c_k+T_3c_{k+1} = -R-t_1c_{i-1}-t_2c_{j-1}. \tag{14}$$

Here the residual R and the coefficients T_1, T_2, T_3, t_1, t_2 are given by

$$R \equiv (1-\mu_{ijk})p_{ijk}+\mu_{i-1,jk}p_{i-1,jk}+q_{ijk}+r_{ijk}$$

$$T_1 \equiv (\Delta z)^{-2},$$

$$T_2 \equiv -(\Delta x)^{-2}\{2\omega^{-1}(1-\mu_i)s_i-2\mu_{i-1}s_{i-1}\}$$
$$-(\Delta y)^{-2}\{2\omega^{-1}(1-\mu_i)+\mu_i\} - 2(\Delta z)^{-2},$$

$$T_3 \equiv (\Delta z)^{-2},$$

$$t_1 \equiv (\Delta x)^{-2}(1-\mu_i)s_i-2\mu_{i-1}s_{i-1},$$

$$t_2 \equiv (\Delta y)^{-2}.$$

The discrete inner problem was fomulated above as a sequence of dense linear systems,

$$A_i S_i = B_i, \quad 1 \le i \le imax, \qquad (15)$$

cf. (11). Due to the compatibility condition (10c) the vectors B_i are solution dependent and must be determined in an iterative fashion. Since (15) thus has to be solved several times with different right hand sides we invert each A_i and save the inverse matrices on secondary storage. A special computation with the boundary condition (10c) omitted and panels along the wing/body perimeter in (10b) only is done to find an initial approximation ψ^0 to ψ.

5. Iterative Coupling Procedure

The coupling between the outer and inner problems is effected by the compatibility conditions (8c) and (10c). We may view the solving of (10) as a procedure for updating the boundary condition (8c). Rather than performing a large number of sweeps according to (14) with ψ fixed in (8c) we use the following strategy:

Step 0: Compute a start approximation ψ^0 as described above and solve (14) for ϕ^* with $\phi=0$.

Step 1: Perform a sequence of relaxation sweeps according to (14) with the normal derivative of ψ on the parallelepiped surface, ψ_n in the boundary condition (8c), updated by solving (15) for each sweep. Proceed until the maximum change in ψ_n from one sweep to the next has decreased by half a decade.

Step 2: Perform a sequence of relaxation sweeps according to (14) keeping ψ_n in (8c) fixed. Proceed until the maximum potential correction cmax from one sweep to the next has decreased by half a decade.

Repeat step 1 and 2 until some stopping criterion is satisfied, typically $cmax < 10^{-4}$.

Updating of the solution dependent boundary conditions (8b) and (8d) is done similarly with the test quantity in step 1 replaced by "maximum change in ϕ_z on the wing surface" and "maximum change in circulation", respectively.

A schematic picture of the iterative solution procedure is given in Figure 5.

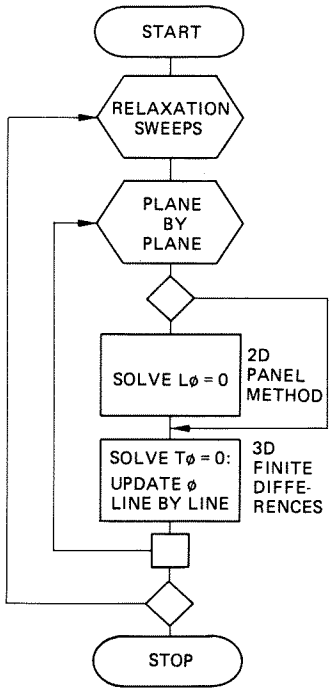

Figure 5. Iteration process.

6. Numerical Computations

We shall use the method described above to compute pressure distributions in transonic flow for three different configurations: an analytically defined bumpy and indented body[12], the RAE wing/body combination[13], and a wing/fuselage fighter configuration which has been wind tunnel tested by SAAB. We also give some results from 2D calculations on a NACA0012 profile to indicate the possible gain in accuracy one can make by using a higher order TSP formulation. The normalized pressure coefficient C_p is computed using the formula

$$C_p = -2\phi_x - (1-M_\infty^2)\phi_x^2 - \phi_y^2 - \phi_z^2 .$$

Computational grids

For each configuration we use a sequence of non-uniform Cartesian computational grids of the type shown in Figure 3, Section 2.

The mean surface of the wing is placed halfway between two horizontal grid planes $z=z_k$ and $z=z_{k+1}$. Vertical grid planes cutting the wing have related spacings in the x- and y-directions so that at each span station $y=y_j$ the x-coordinate of the leading edge is halfway between two grid planes $x=x_i$ and $x=x_{i+1}$. The y-coordinate of the wing tip is halfway between two grid planes $y=y_j$ and $y=y_{j+1}$. The step size Δz across the mean plane of the wing is typically 50% larger than the minimum step size Δx across the leading edge.

The resolution power of each grid is controlled by four parameters setting the relative resolution at the nose of the body, at the body/sting junction, at the wing root leading edge, and at the wing tip leading edge. For the RAE wing/body these parameters were 5%, 5%, 4%, 4%, resulting in 927,000 points for the finest grid. The corresponding data for the fighter configuration was 2%, 5%, 1%, 5%, and 3.4 million points. The results presented for the analytically defined body were obtained on a grid with 45,000 points.

Computed pressure distributions

Results for the analytically defined body is shown in Figure 6. Computed pressures are in good agreement with wind tunnel data. We note that the positive peak in the computed C_p-curve on the indented part of the surface is less pronounced in the wind tunnel data, probably because of viscous boundary layer effects.

Figure 7 shows results for the RAE wing/body combination in a lifting case. We note that the suction peaks on the body surface induced by the presence of the wing are remarkably accurate. In the domain just upstream of the wing the increase in pressure due to flow stagnation is underpredicted. Qualitatively, leaving out the ϕ_{xx} term in the inner problem will have this effect, as can be seen by applying Green's formula to the TSP-equation (5a) inside the parallelepiped P.

The pressure distributions on the RAE wing is given at three different spanwise locations in Figure 7. The agreement between computations and experiments is good and the shock is in its right position. At the wing tip the suction peak is underpredicted due to an insufficient resolution power of the grid in this region. We also note a certain disagreement at the trailing edge close to the body.

Results for the fighter configuration are shown in Figure 8. The fuselage geometry of this wind tunnel model contains some noise since it has been obtained by digitizing from a drawing. Nevertheless, the body pressure signature characterized by the suction peak over the canopy is in good agreement with wind tunnel data. The wing pressures, including shock positions, are accurately described except at the leading edge, where a finer grid is required.

Let us finally remark, that computed pressure distributions on the body surface are of good quality also for the coarse grids. The fine grids are however necessary to produce accurate results on the wing surface. This is in particular so in the leading edge region, where even the finest discretization levels used here have been insufficient to catch the suction peak properly. A requirement of say 0.1% grid size relative to the local chord along a swept leading edge will however result in a tremendous amount of points if a strictly cartesian grid is used. Work is now in progress to allow for local grid refinement to overcome this difficulty.

Convergence history

A sequence of grids was used for each configuration. The solutions on coarse grids served as initial approximations for the fine grids. The stopping criterion was $cmax<10^{-4}$, where cmax denotes the maximum potential correction. For the fighter configuration the convergence was driven further to $cmax<10^{-5}$ with hardly noticable changes in the pressure values.

The convergence history for cmax is shown in Figure 9. When boundary condition updating is activated, as described in Section 5, we get a temporary increase in cmax. During the subsequent iterations, however, cmax decreases rapidly and soon recovers its value prior to the update period.

For the RAE wing/body combination the average reduction factor for cmax was 0.88 and the CPU-time on CRAY-1A was 300 seconds on the finest grid. The corresponding figures for the fighter configuration was 0.85 and 400 seconds (to $cmax=10^{-4}$).

Some 2D results with a higher order TSP method.

The boundary condition (6) in Section 2 includes ϕ_x and ϕ_y terms. In some (standard) TSP formulations these terms are omitted. To improve the accuracy of the TSP formulation further, one can augment the operator T in (3a) by including all perturbation terms of second order with respect to the relative thickness τ_w. The results of these modifications may give a significant improvement as shown in Figure 10.

Conclusions

We have presented a small disturbance formulation for transonic flow computations about wing/fuselage configurations. The concept of the method has been verified and the numerical process is rapidly converging.

Computed pressure distributions on several configurations, including a modern fighter, show good agreement with wind tunnel test data. In particular, wing/body interactions are well described.

Accurate results in the wing leading edge region requires computational grids of high resolution power. Grid point reduction by local grid refinement seems to be an attractive possibility to reduce the computational costs in such cases. So far encouraging results have been obtained for the ONERA M6 wing using a hierarchy of embedded staircase shaped grids along the leading edge.

References

(1) H.Akima, A new method of interpolation and smooth curve fitting based on local procedures, JACM 17(4), pp. 589-602, 1970.

(2) H. Ashley and M. Landahl, Aerodynamics of Wings and Bodies, Addison-Wesley, 1965.

(3) F.R.Bailey, On the computation of two- and three-dimensional steady transonic flows by relaxation methods, VKI Lecture series "Progress in Numerical Fluid Dynamics", 1974.

(4) C.W.Boppe, Transonic Flow Field Analysis for Wing-Fuselage Configurations, NASA CR-3243, 1980.

(5) P.Caap and L.Elmeland, Calculation of static elastic effects on a modern high performance aircraft, AIAA paper 86-1771-CP, San Diego 1986.

(6) K.Fujii and S.Obayashi, Practical Applications of New LU-ADI Scheme for the Three-Dimensional Navier-Stokes Computation of Transonic Viscous Flows, AIAA paper 86-0513, Reno 1986.

(7) A.Jameson, The Evolution of Computational Methods in Aerodynamics, Princeton University MAE Report No. 1608, 1983.

(8) A.Jameson and W.Schmidt, Some Recent Developments in Numerical Methods for Transonic Flows, Computer Methods in Applied Mechanics and Engineering, vol.51, pp. 467-493, 1985.

(9) E.R. Klunker, Contribution to Methods for Calculating the Flow about Thin Lifting Wings at Transonic Speeds. Analytical Expressions for the Far Field, NASA TN D-6530, 1971.

(10) H.W.Liepmann and A.Roshko, Elements of Gasdynamics, John Wiley & Sons, 1957.

(11) E.M.Murman, Analysis of Embedded Shock Waves Calculated by Relaxation Methods, AIAA Journal, vol 12, no 5, pp 626-633, 1974.

(12) R.A.Taylor, Pressure Distributions at Transonic speeds for Bumpy and Indented Midsections of a Basic Parabolic-Arc Body, NASA MEMO 1-22-59A, 1959

(13) D.A.Treadgold, A.F.Jones, and K.H.Wilson, Pressure distribution measured in the RAE 8ft x 6ft transonic wind tunnel on RAE wing 'A' in combination with an axi-symmetric body at Mach numbers of 0.4, 0.8, and 0.9, in AGARD Advisory Report 138, pp. B4:1-25, 1979.

(14) A.Verhoff and P.J.O'Neil, Extension of FLO Codes to Transonic Flow Prediction for Fighter Configurations, in Transonic Aerodynamics, ed. D.Nixon, pp 467-487, AIAA, 1982.

(15) F.A.Woodward, Analysis and design of wing-body combinations at subsonic and supersonic speeds, J. of Aircraft, vol.5, part 6, pp. 528-534, 1968.

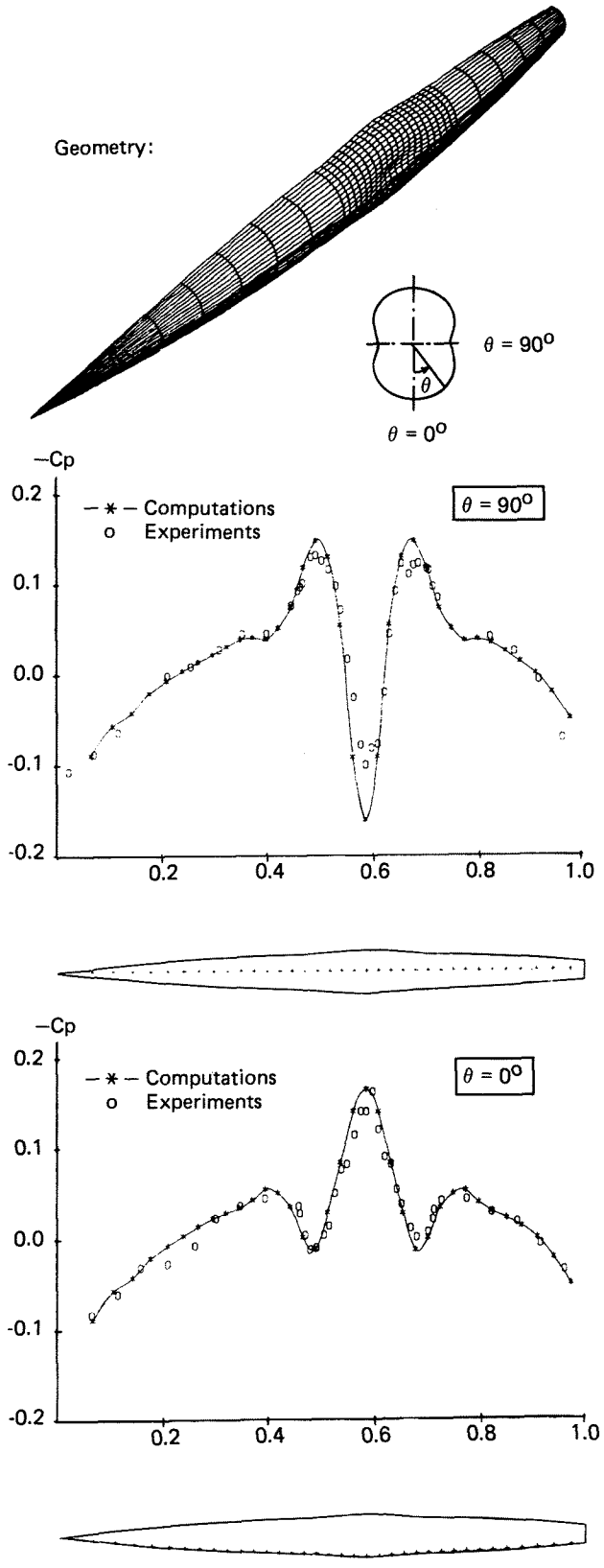

Figure 6. Comparison between computed pressure signatures and wind tunnel data [12] for an analytically defined body at zero angle of attack. The Mach number is $M_\infty = 0.95$.

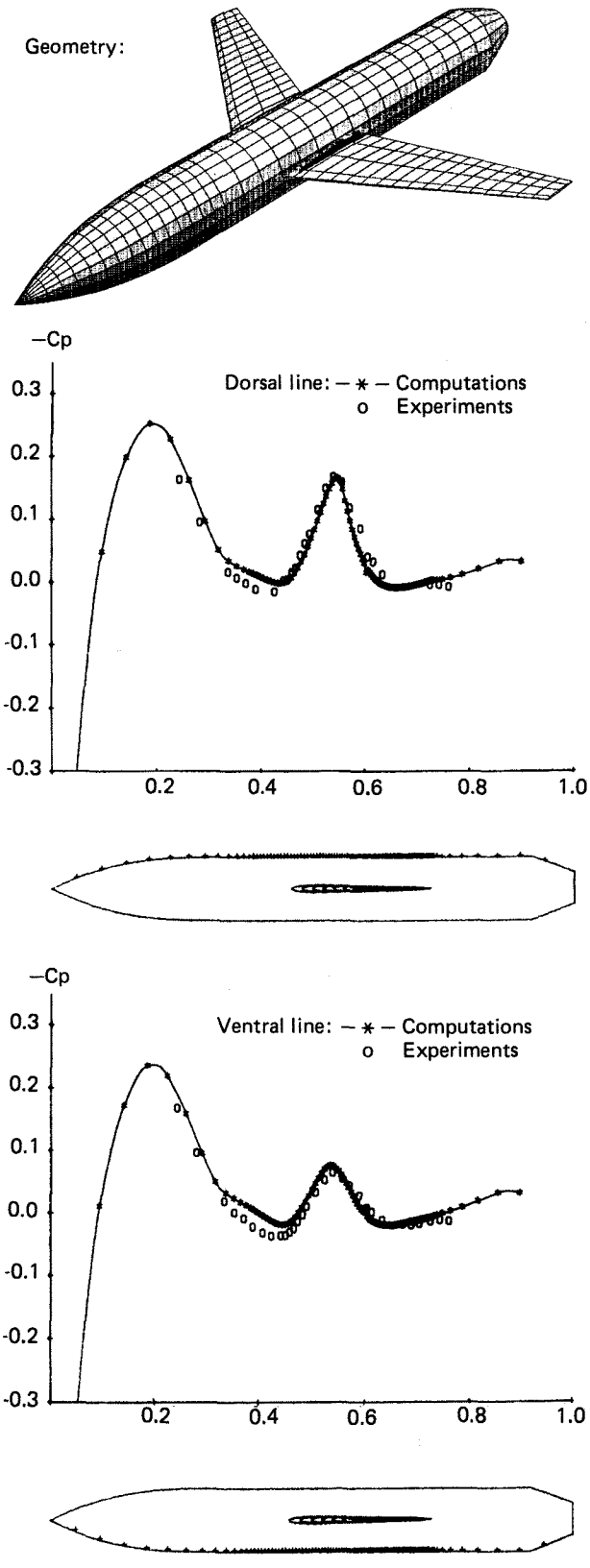

Figure 7. Computed and experimental [13] pressure distributions for the RAE wing/body combination at $M_\infty = 0.90$ and $\alpha = 1^o$, dorsal and ventral line pressures.

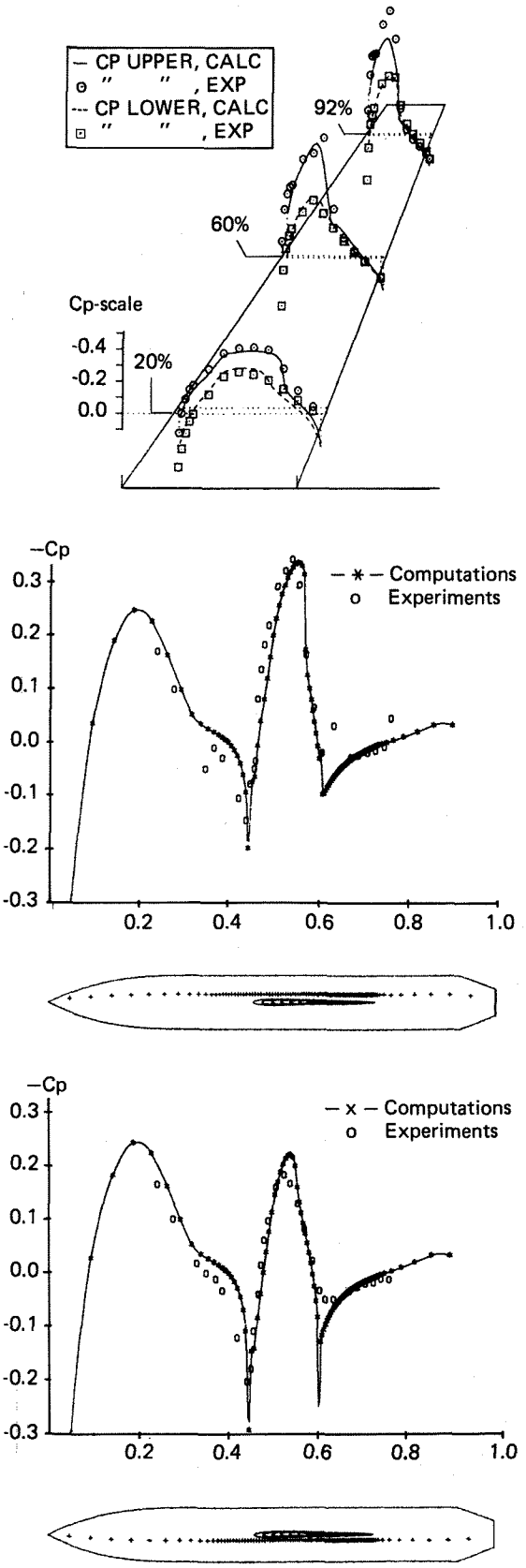

Figure 7. (Continued)
Wing pressures and body pressures above and below the wing for the RAE wing/body.

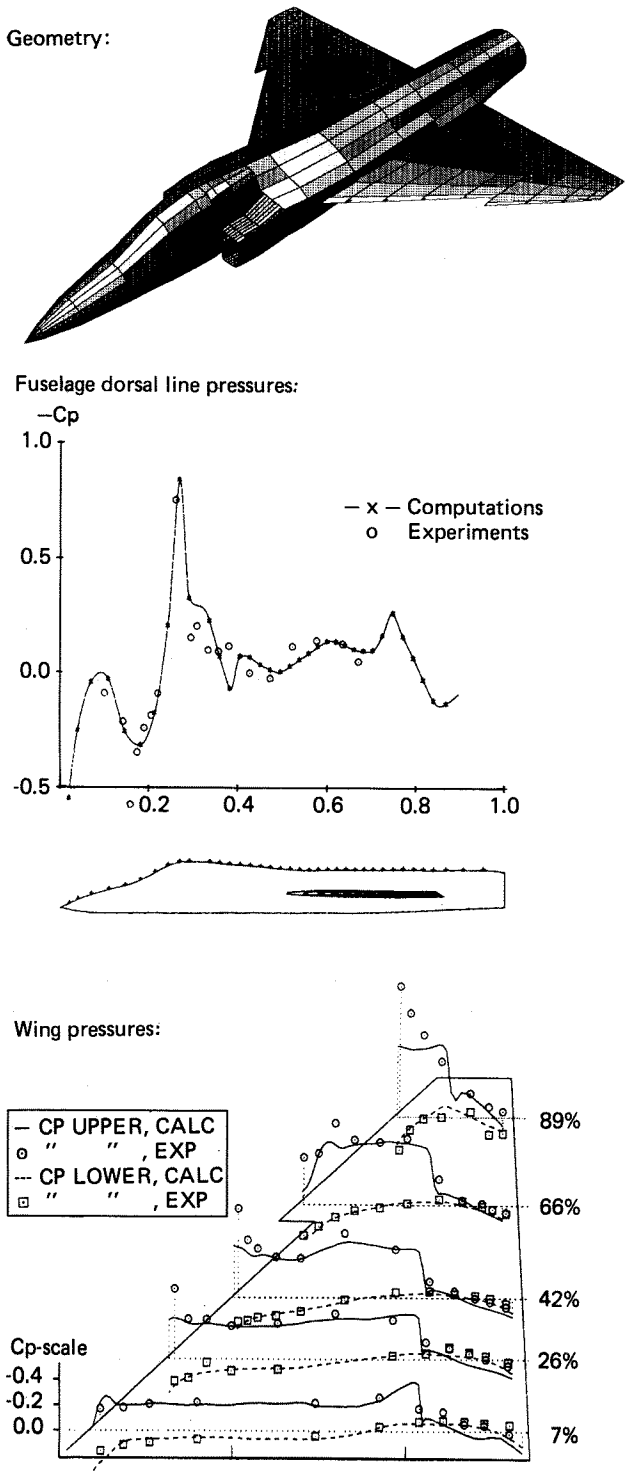

Figure 8. Computed and experimental pressure distributions for a fighter configuration at $M_\infty = 0.92$ and $\alpha = 3.3^o$.

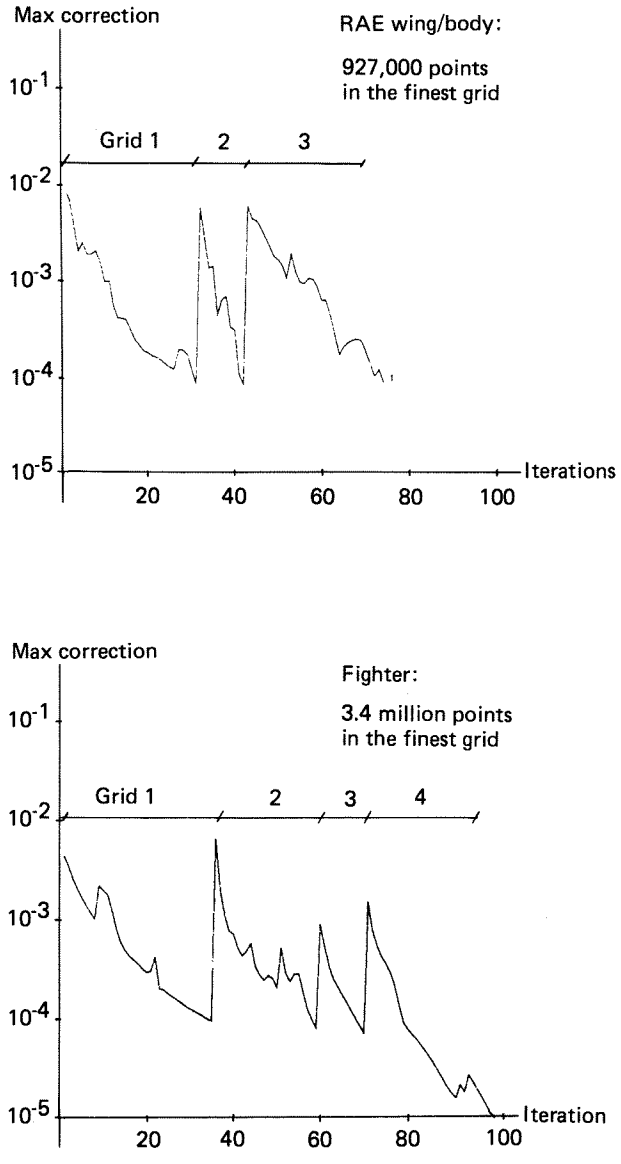

Figure 9. Convergence history for the RAE wing/body combination (top) and a fighter configuration (bottom).

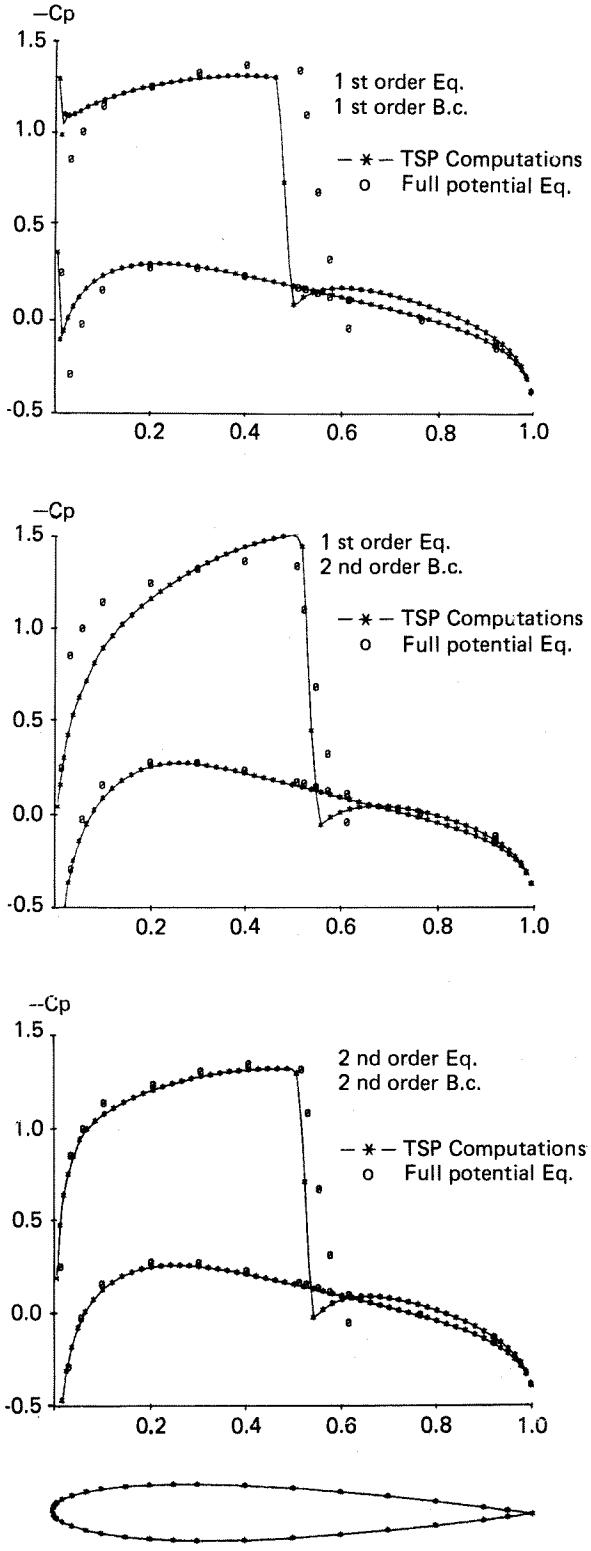

Figure 10. Pressure distributions on a NACA0012 profile at $M_\infty = 0.75$ and $\alpha = 2^o$ computed with different TSP formulations.